International Journal of Nanomedicine

Dovepress

open access to scientific and medical research

Open Access Full Text Article

ORIGINAL RESEARCH

Superhydrophilic PLGA-Graft-PVP/PC Nanofiber Membranes for the Prevention of Epidural Adhesion

Qingxin Fan[1,*], Hao Wu[1,2,*], Qingquan Kong[1]

[1]Department of Orthopedics, Orthopedic Research Institute, West China Hospital, Sichuan University, Chengdu, People's Republic of China; [2]Department of Orthopedics, The Second Affiliated Hospital of Dalian Medical University, Dalian, People's Republic of China

*These authors contributed equally to this work

Correspondence: Qingquan Kong, Department of Orthopedics, Orthopedic Research Institute, West China Hospital, Sichuan University, Chengdu, 610041, People's Republic of China, Email kqqspine@126.com

Background: The frequent occurrence of failed back surgery syndrome (FBSS) seriously affects the quality of life of postoperative lumbar patients. Epidural adhesion is the major factor in FBSS.

Purpose: A safe and effective antiadhesion material is urgently needed.

Methods: A superhydrophilic PLGA-g-PVP/PC nanofiber membrane (NFm) was prepared by electrospinning. FTIR was performed to identify its successful synthesis. Scanning electron microscopy, thermogravimetric analysis, differential scanning calorimetry, and water contact angle measurement were performed. CCK-8 assays were performed in primary rabbit fibroblasts (PRFs) and RAW264.7 cells to explore the cytotoxicity of PLGA-g-PVP/PC NFm. Calcein-AM/PI staining was used to measure the adhesion status in PRFs. ELISA was performed to measure the concentrations of TNF-α and IL-10 in RAW264.7 cells. In addition, the anti-epidural adhesion efficacy of the PLGA-g-PVP/PC NFm was determined in a rabbit model of lumbar laminectomy.

Results: The PLGA-g-PVP/PC NFm exhibited ultrastrong hydrophilicity and an appropriate degradation rate. Based on the results of the CCK-8 assays, PLGA-g-PVP/PC NFm had no cytotoxicity to PRFs and RAW264.7 cells. Calcein-AM/PI staining showed that PLGA-g-PVP/PC NFm could inhibit PRF adhesion. ELISAs showed that PLGA-g-PVP/PC NFm could attenuate lipopolysaccharide-induced macrophage activation. In vivo experiments further confirmed the favorable anti-epidural adhesion effect of PLGA-g-PVP/PC NFm and the lack of a strong inflammatory response.

Conclusion: In this study, PLGA-g-PVP/PC NFm was developed successfully to provide a safe and effective physical barrier for preventing epidural adhesion. PLGA-g-PVP/PC NFm provides a promising strategy for preventing postoperative adhesion and has potential for clinical translation.

Keywords: superhydrophilic membrane, irradiation graft, postoperative adhesion, failed back surgery syndrome, electrospinning

Introduction

As the population ages and sedentary lifestyles increase dramatically, the prevalence of degenerative lumbar spine disease is increasing. Surgical decompression can relieve the compression of nerve roots or the spinal cord by degenerative tissues and palliate the clinical symptoms.[1] However, the frequent occurrence of failed back surgery syndrome (FBSS, 4% ~ 48%) seriously affects the quality of life of postoperative patients.[2] Epidural adhesion is considered the most common cause of FBSS and involves various degrees of inflammatory infiltration, scar tissue formation, and tissue adhesions in the epidural space.[3] Although improved surgical methods and drug therapy regimens can exert a degree of control over FBSS, they have limited clinical effects.[4] Recently, with advances in nanomaterials, antifibrotic nanofiber membranes (NFm) have been used to cover the spinal dura mater as a barrier, offering a reliable therapeutic option for halting epidural adhesion and reducing the risks of developing FBSS events.

Received: 29 December 2021
Accepted: 15 March 2022
Published: 25 March 2022

Electrospinning is the most efficacious process for nanofiber production. The spinning solution forms a jet termed a "Taylor cone" under the effect of a strong electric field. The solvent is evaporated during spinning solution ejection, and the solute falls on a collector to form the NFm.[5] Due to close contact with the dura mater and peripheral nerve roots, distinctive properties are required for an antifibrotic NFm: 1. effective inhibition of the adhesion of fibroblasts and prevention of epidural adhesion; 2. good biocompatibility to maintain microenvironment stability around the nerve roots and spinal cord; and 3. appropriate degradability to reduce the risk of infection.

Poly (lactic-co-glycolic acid) (PLGA) is a common high-molecular-weight polymer with good biocompatibility and degradability and has been approved by the US Food and Drug Administration (FDA).[6,7] PLGA can be degraded under physiological conditions independent of immune activity, and its degradation rate can be tuned over a broad range by adjusting the molar ratio of lactic acids and glycolic acids.[8] However, PLGA NFm shows low hydrophilicity, and its degradation products can decrease the pH of the surrounding environment, trigger inflammation and accelerate adhesion formation.[9–11] Accordingly, PLGA NFm requires modification. Polymerization with other polymers is a common modification method. Li et al reported a chitosan-covalent PLGA (CS-graft-PLGA) nanofiber and found that the addition of CS could improve the hydrophilicity, mechanical properties, degradation rate and protein adsorption of PLGA nanofibers.[12] To mimic natural extracellular matrices (ECMs) in vitro, Foraida et al conjugated elastin with PLGA and fabricated elastin-covalent PLGA nanofibers. They found that conjugation with elastin improved the hydrophilicity and stretchability compared with PLGA nanofibers.[13] Kazemi et al conjugated polyethylene glycol (PEG) with PLGA and cultured neurogenic tumor cells in PEG-covalent PLGA (PEG/PLGA) nanofibers. The in vitro results suggested that PEG/PLGA nanofibers had excellent hydrophilicity, anti-inflammatory properties and safety, and the addition of PEG could decrease the thickness of PLGA nanofibers.[14]

Polyvinylpyrrolidone (PVP), which has also been approved by the FDA, is a high-molecular-weight polymer formed by the self-polymerization of N-vinylpyrrolidone (NVP).[15] Wang et al used 60Co-γ to graft NVP onto PLGA to form NVP-covalent PLGA, which is a safe method of great interest.[16] Subsequently, Wang et al prepared PLGA-g-PVP/I electrospun fibrous membranes using the same method, and the results were outstanding in preventing postoperative abdominal adhesion.[17] However, PVP/I is an irritant for mucous membranes, although this effect is not strong. Unfortunately, because an anti-epidural adhesion NFm is immediately adjacent to the nerve roots and spinal cord, even mild inflammation can provoke overt clinical manifestations, and a functional and safer biomaterial is needed. Phosphatidylcholine (PC) is a surfactant that usually acts as a lubricant to smooth the membrane surface and prevent secondary damage. Its antiadhesion effect has been well documented in abdominal surgery and is not affected by intraoperative bleeding or bacterial infections.[18] Because of these features, PC is a superior candidate for antiadhesion.

Therefore, gamma rays were used to graft PVP to PLGA (PLGA-g-PVP), and PLGA-g-PVP/PC NFm was made by electrospinning after physically mixing the PLGA-g-PVP solution with the PC solution. First, the morphology, composition, thermal stability, hydrophilicity, and degradation rate of the PLGA-g-PVP/PC NFm were identified. Second, we explored the cytotoxicity, biocompatibility, and anti-cell adhesion ability of PLGA-g-PVP/PC NFm in vitro. The results showed that PLGA-g-PVP/PC NFm barely affected the activity of fibroblasts and macrophages, did not activate inflammation, and reduced the number of adhered cells in the coculture system of fibroblasts and NFm. In addition, PLGA-g-PVP/PC NFm showed excellent anti-epidural adhesion effects. This Research provides a new strategy for optimizing the design of highly safe anti-scar adhesion materials (Scheme 1).

Materials and Methods

Materials

PLGA (75:25) was purchased from Shandong University (Jinan, China). NVP, PC, DMF, chloroform, and lipopolysaccharide were purchased from Aladdin Industrial Corporation (Shanghai, China). New Zealand rabbits were provided by the West China Animal Laboratory Center of Sichuan University (Sichuan, China). Raw264.7 cells were provided by Cybertron Medical Technology Co. (Beijing, China). Collagenase II, DAPI, CCK-8, and the Mouse TNF-α/IL-10 ELISA Kit were purchased from Beijing Soledad Bao Technology Co. (Beijing, China). The anti-vimentin Ab, anti-TNF-α Ab,

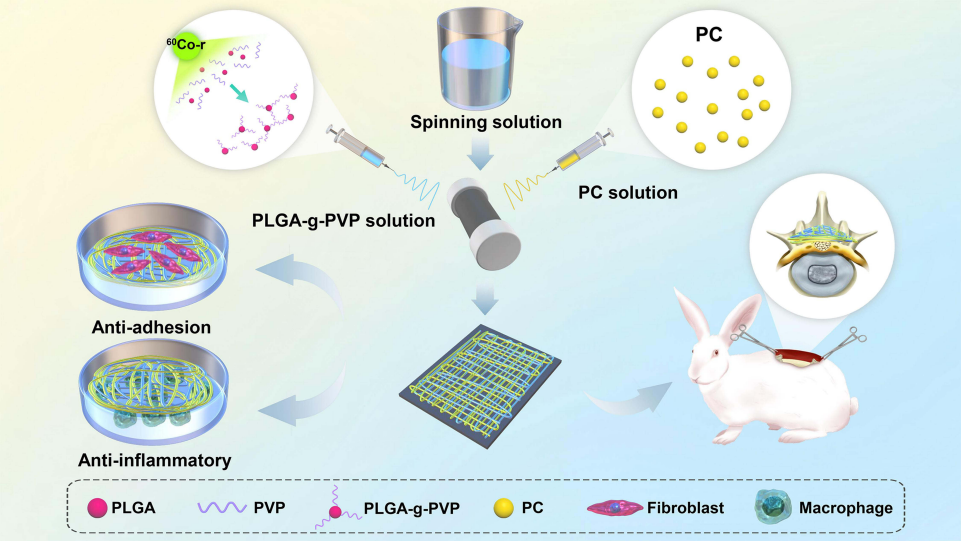

Scheme 1 Schematic illustration of the preparation of PLGA-g-PVP/PC NFm and the antiadhesion and anti-inflammatory assays in vivo and in vitro.
Abbreviations: PLGA, poly (lactic-co-glycolic acid); PVP, polyvinylpyrrolidone; PC, phosphatidylcholine.

anti-IL-6 Ab, and FITC-conjugated secondary antibody were purchased from Biolegend. Calcein-AM/PI was purchased from Biyuntian Biotechnology (Shanghai, China).

Fabrication of PLGA-g-PVP/PC NFm

First, PLGA-g-PVP powders were prepared. PLGA (100 g) was dissolved in methanol (150 mL) to produce solution A, and NVP (50 mL) was fully mixed with solution A to produce solution B. Solution B was transferred to a round-bottom flask, bubbled with nitrogen to adequately remove oxygen, and sealed in a bottle mouth. The sealed round-bottom flask was irradiated with 60Co-γ (2.5 kGy/h, 2 h) at room temperature to copolymerize NVP with PLGA, and PLGA-g-PVP powders were obtained. To improve the purity of the PLGA-g-PVP particles, the precipitates were ultrasonically cleaned, soaked in ethanol for 24 h at room temperature, and dried in vacuum at 37 °C.

Second, PLGA-g-PVP/PC NFm was prepared. PLGA-g-PVP (1.5 g) was dissolved in 10 mL of spinning solution (chloroform: DMF, *1:1, v/v*) to prepare PLGA-g-PVP solution. Then, 100 mg or 500 mg of PC was dissolved in 10 mL of spinning solution to prepare solution PC1 or PC2, respectively. Solutions PLGA-g-PVP and PC were simultaneously ejected from the needle (25G) and formed two interwoven "Taylor cones", which formed the NFm (Scheme 1). The fabrication parameters of each group are described in Table 1.

Characterization of the PLGA-g-PVP/PC NFm

The ATR-FTIR spectra of PLGA NFm, PLGA-g-PVP NFm, and PLGA-g-PVP/PC NFm were obtained on a Nicolet iS 10 (Thermo Fisher Scientific, USA). Scanning electron microscopy (SEM) images were taken from FEI Inspect-F (Philips, the Netherlands). Thermogravimetric analysis (TGA) and differential scanning calorimetry (DSC) were carried out on a TGA Q50 (TA Instruments, USA) and DSC Q2000 (TA Instruments, USA), respectively. The water contact angle (WCA) was determined with DataPhysics (DataPhysics, Germany). A small piece of NFm was taken, and the dry weight was recorded (W0). Then, the NFm was soaked in PBS until saturated, and the wet weight was recorded (W1). The water absorption was evaluated by the following formula: Water absorption (%) = [(W1 – W0)/W1] × 100%. The NFm was soaked in PBS at 37 °C and shaken at 600 rpm. The dry weight (W2) was recorded at 7, 14, 21, and 28 days, and the degradation rate of NFm was evaluated by the following formula: residual weight ratio (%) = (W2/W0) × 100%.

Table 1 Electrospinning Parameters

Group	Thickness (mm)	Voltage (kV)		Tip-to-Collector Distance (mm)		Feed Rate (mL/h)		Time (h)
		PLGA-g-PVP	PC			PLGA-g-PVP	PC	
PLGA	1	12	/	120	/	1.2	/	48
	2							96
PLGA-g-PVP	1	14	/	160	/	1.2	/	48
	2							96
PLGA-g-PVP-PC1	1	14	16	200	200	1.2	1.0	48
	2							96
PLGA-g-PVP-PC2	1	14	18	200	200	1.2	1.0	48
	2							96

Abbreviations: FBSS, failed back surgery syndrome; NFm, nanofiber membrane; PLGA, poly (lactic-co-glycolic acid); FDA, Food and Drug Administration; ECMs, extracellular matrices; PEG, polyethylene glycol; PVP, poly-vinylpyrrolidone; NVP, N-vinylpyrrolidone; PC, phosphatidylcholine; SS, spinning solution; SEM, scanning electron microscope; TGA, thermogravimetric analysis; DSC, differential scanning calorimetry; WCA, water contact angle; PRFs, primary rabbit fibroblasts; IF, immunofluorescence; ROS, reactive oxygen species; H&E, hematoxylin-eosin.

Extraction and Identification of Primary Rabbit Fibroblasts (PRFs)

PRFs were established by the method of differential adhesion.[19] Briefly, the paraspinal muscles of rabbits were dissociated and washed with PBS to remove the blood. The tissue was cut into pieces and digested with 0.1% collagenase II at 37 °C for 2 hours, then passed through a 150-mesh screen. The filtrate was collected and centrifuged at 1000 rpm for 10 min. The supernatant was discarded, and the cells were resuspended at 1×10^5/mL in complete medium, seeded in 10 cm dishes, and cultured in an incubator.

PRFs were identified by immunofluorescence (IF) staining of vimentin, and IF staining was performed as previously described.[20] Briefly, the cells were permeabilized with 0.2% Triton for 10 min after fixation with 4% paraformaldehyde at 4 °C for 30 min. Primary antibodies against vimentin (1:100) and FITC fluorescence secondary antibody (1:500) were used to visualize the expression of vimentin, and DAPI was used to label the cell nuclei. Images were taken on a DM IRB microscope (Leica, Italy).

Cytotoxicity

A total of 5×10^5 PRFs or RAW264.7 cells were seeded into 6-well plates to 70–80% confluence. Each NFm was cropped into a circular piece (diameter = 30 mm and thickness = 2 mm), sterilized for 2 min under UV light, and cocultured with cells. CCK-8 was used to test cell viability at 24 hours according to the manufacturer's instructions.

Fibroblast Adhesion

UV-sterilized NFm (diameter = 20 mm and thickness = 2 mm) was placed at the bottom of 12-well plates, and 1×10^5 PRFs were seeded into each well. The medium was discarded on days 1, 3, and 5, and the NFm was washed with PBS and submerged in calcein-AM/PI solution at 37°C for 15 min. The adhesion number and state of fibroblasts were detected by an inverted fluorescence microscope.

Inflammatory Reaction in vitro

RAW264.7 cells (1×10^5) were seeded into 24-well plates to 70–80% confluence and cultured with UV-sterilized NFm (diameter = 30 mm and thickness = 1 mm) and lipopolysaccharide (1 μg/mL) for 24 h. The supernatant was collected for TNF-α and IL-10 measurements by ELISA.

Establishment of the Surgical Model

Lumbar laminectomy of rabbits was used to emulate decompressive surgery. Three-month-old New Zealand rabbits (n = 45) were randomly divided into 3 groups, NFm was inserted after laminectomy. After fasting for 24 h, rabbits were anesthetized with Sumianxin II (0.1 mL/kg, intramuscular) and phenobarbital sodium (1.1 mL/kg, intravenous injection).

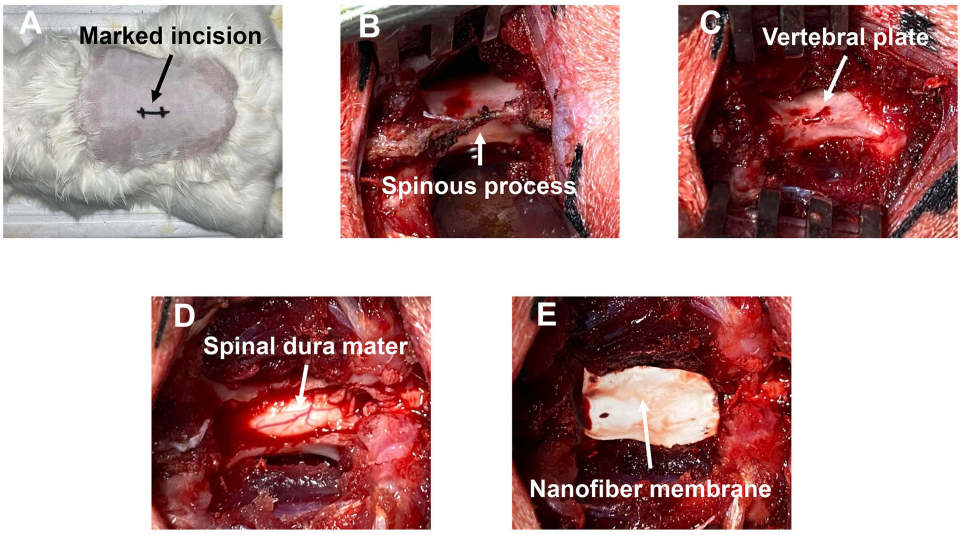

Scheme 2 Modeling process. (**A**) Preoperative preparation of the incision site; (**B**) exposed lamina; (**C**) removed spinous process; (**D**) removed lamina; (**E**) spinal dura mater covered by NFm.

The skin surrounding L5 was prepared and disinfected with povidone-iodine. Skin, fat, fascia, and muscle were separated layer by layer to expose the vertebral plate. The L5-related supraspinous ligament, spinous process, and ligamentum flavum were successively cut, and the vertebral plate was isolated to expose the spinal dura mater. The NFm was placed to completely cover the spinal dura mater after adequate hemostasis. The incision was sutured layer by layer, and penicillin (2×10^5 units/kg, intramuscular) was administered to prevent infection (Scheme 2).

Adhesion Evaluation

After anesthesia, rabbits were sacrificed by air embolization on days 7, 14, 21, and 28. The epidural adhesion and scar tissue along the incision site were exposed. The adhesion strength was evaluated by the Rydell & Balazs method: 0, no obvious adhesion; 1, slight adhesion; 2, extensive and tight adhesion; and 3, severe adhesion, and release of the adhesion disrupted the integrity of the spinal dura mater.

Histological and Immunohistochemistry Analyses

Rabbits were killed on day 28, and scar tissues were separated and fixed. The tissues were embedded in paraffin and sectioned, and the sections were used for H&E staining, picric acid-Sirius red staining, and immunohistochemistry (TNF-α and IL-6). Images were obtained with an Eclipse TE300 inverted microscope (Nikon, Japan).

Statistical Analysis

All data are shown as the mean ± standard deviation. One-way analysis of variance (ANOVA), Fisher's least significant difference, Bonferroni correction for multiple comparisons, and Student's *t*-test were performed using GraphPad Prism v8.1.1 software. The threshold for indicating a statistically significant difference was set to $p < 0.05$.

Results

FTIR Analysis of PLGA-g-PVP/PC NFm

To judge the successful preparation of PLGA-g-PVP/PC NFm, ATR-FTIR was performed. Each spectrum at 1090 cm^{-1} and 1185 cm^{-1} had two sharp peaks, which originated from the stretching vibrations of the C-O and C-O-C peaks, respectively. In the range of 1730 cm^{-1} to 1780 cm^{-1}, a relatively strong and sharp peak originated from the stretching vibrations of C=O bonds. In addition, there was a small peak in the range of 2920 cm^{-1} to 2950 cm^{-1}, which was characteristic of the stretching vibrations of C–H. These were the characteristic peaks of PLGA.[21,22] Compared to the

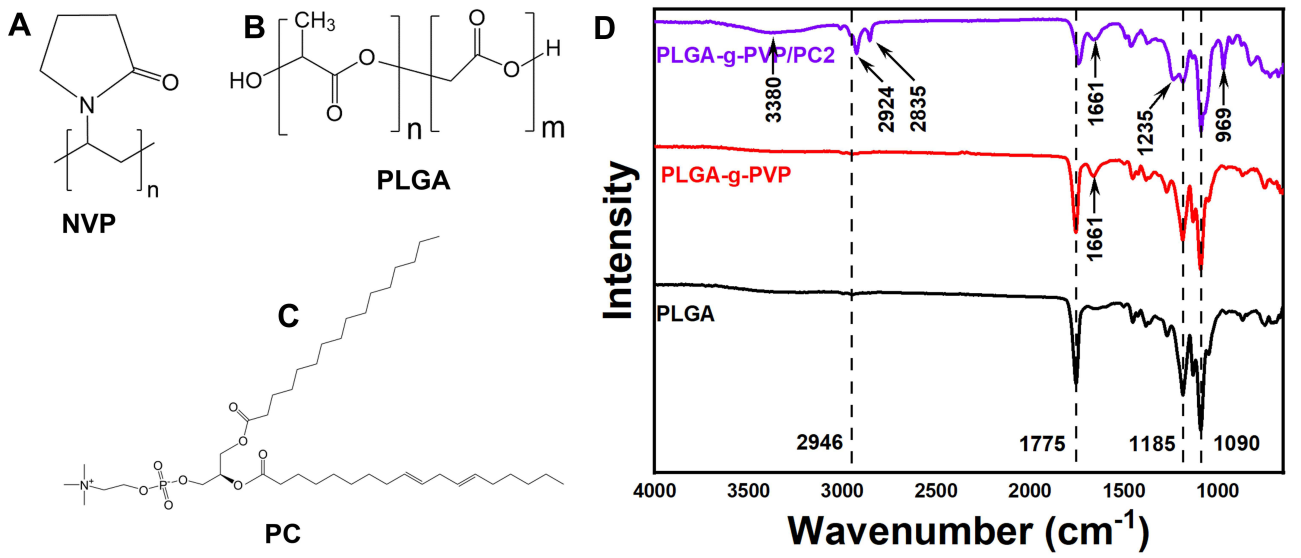

Figure 1 The chemical structural formulas of NVP (**A**), PLGA (**B**), and PC (**C**). (**D**) FTIR spectra of PLGA NFm, PLGA-g-PVP NFm, and PLGA-g-PVP/PC2 NFm.

spectrum of PLGA, the spectra of PLGA-g-PVP and PLGA-g-PVP/PC revealed a small peak at 1661 cm^{-1}, which originated from the stretching vibrations of C=O bonds and indicated the successful grafting of PVP.[23] Compared to the spectrum of PLGA-g-PVP, the spectrum of PLGA-g-PVP/PC presented more characteristic peaks, which might be caused by the chemical bonding diversity in PC. The peaks of PLGA-g-PVP/PC included a small band at 3380 cm^{-1}, which was related to the asymmetric stretching vibrations of NH2 bonds. Additionally, the bands at 2924 cm^{-1} and 2835 cm^{-1} were attributed to the CH2 bonds of PC. Moreover, bands located at 1235 cm^{-1} and 969 cm^{-1} were observed and assigned to the stretching vibrations of P=O bending and -COOH twisting (Figure 1D). These results indicated the successful synthesis of PLGA-g-PVP/PC.[24]

TEM Analysis of PLGA-g-PVP/PC NFm

After confirming the successful preparation of PLGA-g-PVP/PC, the physicochemical characteristics of each NFm were identified. In this study, four NFms (PLGA, PLGA-g-PVP, PLGA-g-PVP/PC1, and PLGA-g-PVP/PC2) were prepared. The PLGA NFm and PLGA-g-PVP NFm were white, while the PLGA-g-PVP/PC1 NFm and PLGA-g-PVP/PC2 NFm were pale yellow. Compared with the other NFms, the PLGA NFm was the most brittle, while PLGA-g-PVP/PC2 NFm was the softest and had the smoothest surface (Figure 2A). These results indirectly confirmed the successful loading of PVP and PC, and these modifications made the NFm more appropriate for covering the spinal dura mater. The SEM images of all NFms revealed a smooth fiber surface, but PLGA-g-PVP/PC NFm exhibited bead formation (Figure 2B). The fiber diameters were 468.68 ± 139.02 nm, 462.05±135.96 nm, 649.61±137.37 nm, and 669.64±146.70 nm for PLGA, PLGA-g-PVP, PLGA-g-PVP/PC1 and PLGA-g-PVP/PC2 NFms, respectively, using ImageJ software for analysis (Figure 2C).

TGA-DSC Analysis of PLGA-g-PVP/PC NFm

The thermal stability of NFms is very important for understanding their application capabilities. All block copolymers obtained were analyzed by TGA to determine their thermal stability. Between 25 °C and 180 °C, PLGA-g-PVP NFm, PLGA-g-PVP/PC1 NFm and PLGA-g-PVP/PC2 NFm experienced a small loss of mass (Figure 3A–D), possibly due to the evaporation of adsorbed water.[25] PVP and PC are excellent water-absorbing materials, and they significantly increased the wettability of PLGA NFm in our subsequent experiments. The major mass loss of each NFm group occurred between 200 °C and 500 °C. In this range, the masses of PLGA NFm, PLGA-g-PVP NFm, PLGA-g-PVP/PC1 NFm, and PLGA-g-PVP/PC2 NFm decreased by 97.3%, 94.17%, 84.96% and 83.94%, respectively, which could be attributed to the decomposition of carboxyl groups (-COOH) and ester groups (-COOR). Above 500 °C, the mass of each

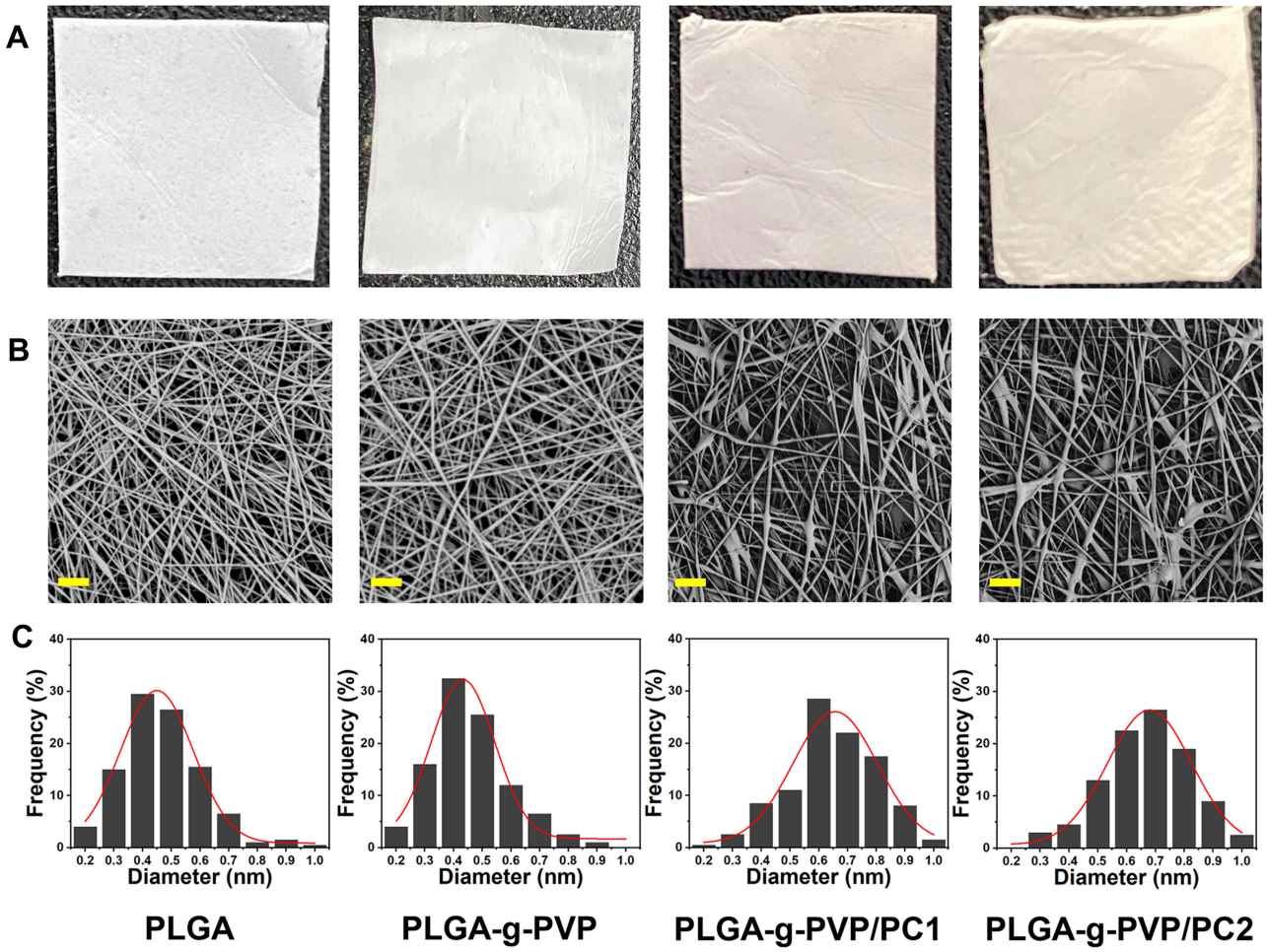

Figure 2 Photographic images (**A**) and SEM images (**B**) of prepared PLGA NFm, PLGA-g-PVP NFm, PLGA-g-PVP/PC1 NFm and PLGA-g-PVP/PC2 NFm (Bar = 10 μm). (**C**) The diameter distribution of each NFm group.

group tended to level off. As shown by DSC, T_{max} was improved from 304 °C for PLGA NFm to 359 °C, 368 °C, and 383 °C for PLGA-g-PVP NFm, PLGA-g-PVP/PC1 NFm, and PLGA-g-PVP/PC2 NFm, respectively (Figure 3A–D). These results indicated that the addition of PVP and PC increased the thermal stability of PLGA NFm.

The Hydrophilicity and Water Uptake Capacity of PLGA-g-PVP/PC NFm

WCA assays were performed on each group to determine the hydrophilicity of the membrane surface. Ten seconds after a 2 μL drop of deionized water was placed on the membrane surface, the WCA was photographed and calculated. WCA assays were performed on each group to determine the hydrophilicity of the membrane surface (Figure 4A). The WCAs were 113.06 ± 5.41°, 44.76 ± 11.80°, 11.05 ± 3.03°, and 7.38 ± 1.13° on the PLGA, PLGA-g-PVP, PLGA-g-PVP/PC1 and PLGA-g-PVP/PC2 NFm surfaces, respectively (Figure 4B). This result implies the ultrastrong hydrophilicity of PLGA-g-PVP/PC. Moreover, PLGA-g-PVP/PC showed good water absorption performance (Figure 4C).

The Degradation Behavior of PLGA-g-PVP/PC NFm

To reduce the risk of infection by implants, appropriate degradation was also needed.[26] During wound repair at the surgical site, the tissue undergoes the inflammatory phase and the new tissue formation phase within 4 weeks. Preventing collagen cross-linking during this time can effectively improve scar adhesion.[27] Therefore, we explored the degradation of NFm in each group in vitro for 4 weeks. The results exhibited varying degrees of mass loss with exposure time. After the 4th week, the residual weight ratios were 81.13 ± 0.52%, 59.57 ± 17.47%, 35.75 ± 9.35, and

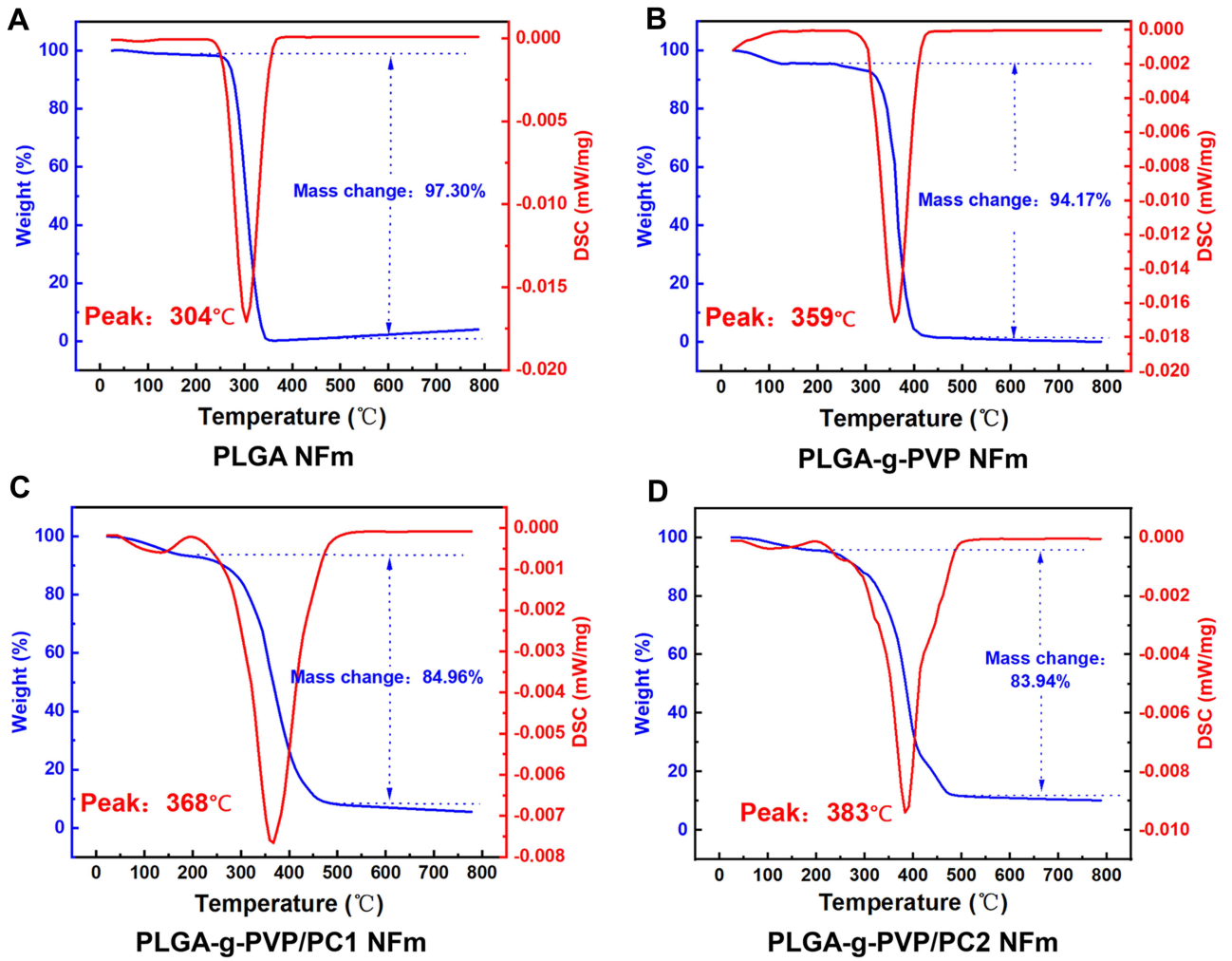

Figure 3 Thermogravimetric analysis results showing different thermal stabilities of PLGA (**A**), PLGA-g-PVP (**B**), PLGA-g-PVP/PC1 (**C**), and PLGA-g-PVP/PC2 (**D**) NFm.

25.81 ± 4.14% for PLGA NFm, PLGA-g-PVP NFm, PLGA-g-PVP/PC1 NFm and PLGA-g-PVP/PC2 NFm, respectively (Figure 4D). The formation of collagen fibers is an important mechanism of postoperative adhesions.[28] Fibroblasts migrate into damaged tissues and secrete collagen 48–72 h after injury, reaching a peak at one week. Collagen is the major component of collagen fibers, which bridge damaged and undamaged tissues.[29] PLGA-g-PVP/PC NFm could present a physical barrier to prevent the formation of this bridge during this time. The results also showed that PLGA-g-PVP/PC NFm had good degradation, and the degradation rates correlated well with the PC content. In contrast to nondegradable material,[30] PLGA-g-PVP/PC NFm appear to reduce the risk of foreign body response and implant infection.

Cytotoxicity Evaluation in vitro

Fibroblasts and macrophages are important in wound healing, and their injury can accentuate the inflammatory response and prolong damage repair.[31] To evaluate the viability impacts of PLGA-g-PVP/PC NFm on PRFs and RAW264.7 cells in vitro, a CCK-8 assay was performed. First, IF staining results showed that vimentin was abundantly expressed in primary cells, which ensured that the PRF extraction was successful (Figure 5A). The results of the CCK-8 assay showed that PLGA-g-PVP/PC NFm had no obvious effects on PRF (Figure 5B) and RAW264.7 cells (Figure 5C) viability. These results indicated that PLGA-g-PVP/PC NFm could prevent cytotoxicity-induced inflammatory responses and enable the NFm to better serve as a safe physical barrier.

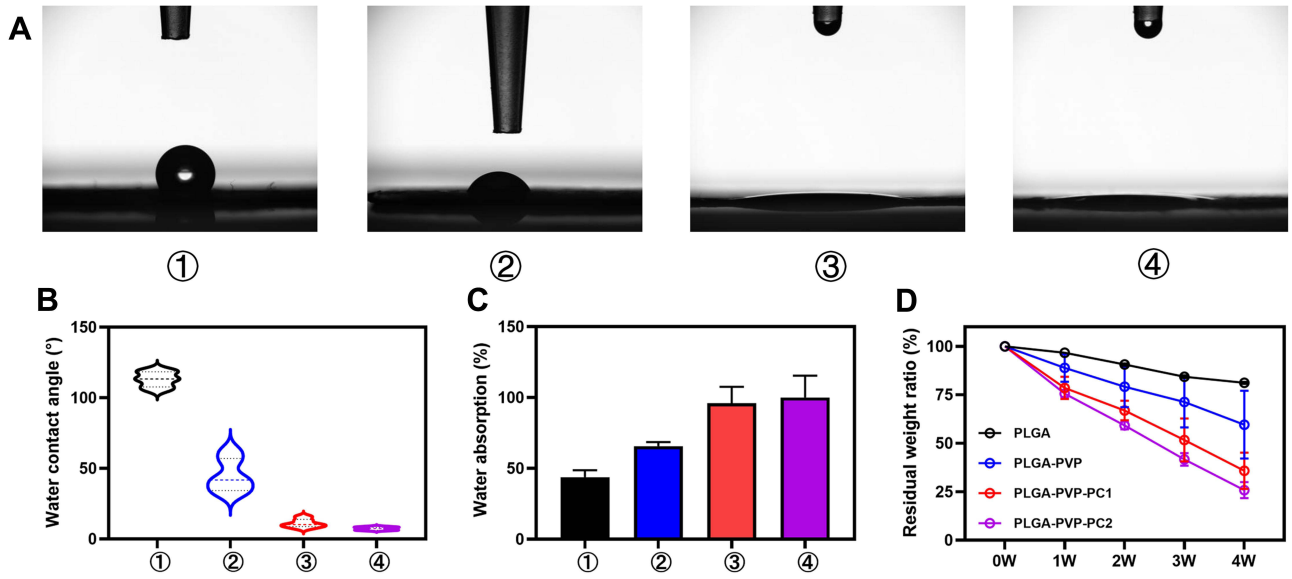

Figure 4 (**A**) A water droplet was photographed after dropping onto each NFm surface group for 10s. (**B**) Water contact angle. (**C**) Water absorption capacity. (**D**) The degradation of each NFm group at different time points (1, 2, 3, and 4 weeks) under simulated physiological conditions (PBS at 37 °C). ①, PLGA NFm; ②, PLGA-g-PVP NFm; ③, PLGA-g-PVP/PC1 NFm; ④PLGA-g-PVP/PC2 NFm.

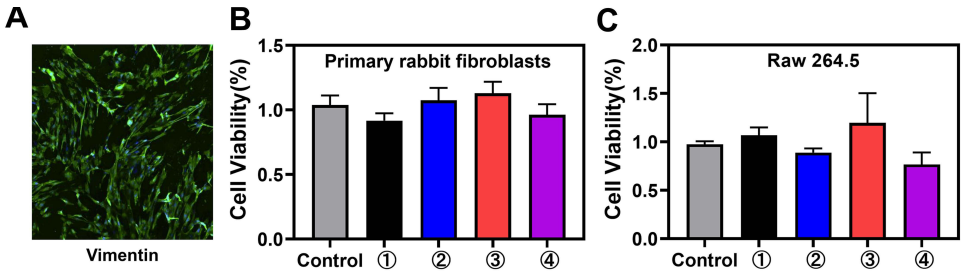

Figure 5 (**A**) The expression of vimentin in PRFs under a fluorescence microscope. Viability of PRFs (**B**) and RAW264.7 cells (**C**) incubated with each NFm group after 24 h. ①, PLGA NFm; ②, PLGA-g-PVP NFm; ③, PLGA-g-PVP/PC1 NFm; and ④, PLGA-g-PVP/PC2 NFm.

The Antiadhesion Effect in vitro

Decreasing the number of adherent fibroblasts on the nanofiber surface is favorable for suppressing adhesion formation. To test the adhesion capacity of fibroblasts, each NFm group was cocultured with PRFs, and the living cells were visualized with calcein-AM/PI on days 1, 3, and 5. The results showed fewer PRFs on the PLGA-g-PVP/PC2 NFm than on other NFms, and the number decreased with increasing PC content (Figure 6A). This indicated that PC could efficiently suppress fibroblast adhesion, which was consistent with the findings of a previous study.[18] This may be because PC significantly decreases the protein adsorption of nanofibers. Zahran et al found that the protein adsorption of PVP electrospun fibers was significantly decreased with increased PC content (0–2%, w/v), and PVP nanofibers hardly adsorbed protein when the content of PC reached 2% (w/v).[32] Superhydrophilicity might also contribute to the prevention of fibrillar adhesion. Traditional antiadhesion membranes are mainly hydrophobic materials, while superhydrophilic materials have been found in recent years to inhibit cell adhesion.[33] In addition, nanoscale topography appears to play a more important role in cell adhesion than the hydrophilic/hydrophobic properties. Zangi et al found that smooth nanoscale topography could significantly suppress cell adhesion,[34] and such cell-repellent behavior is widely used in biosensors and blood-contacting devices. Combined with the results of the CCK-8 assay, PLGA-g-PVP/PC2 NFm clearly had a favorable safety profile and biocompatibility, and the antiadhesion property was primarily dependent on material properties rather than cytotoxicity.

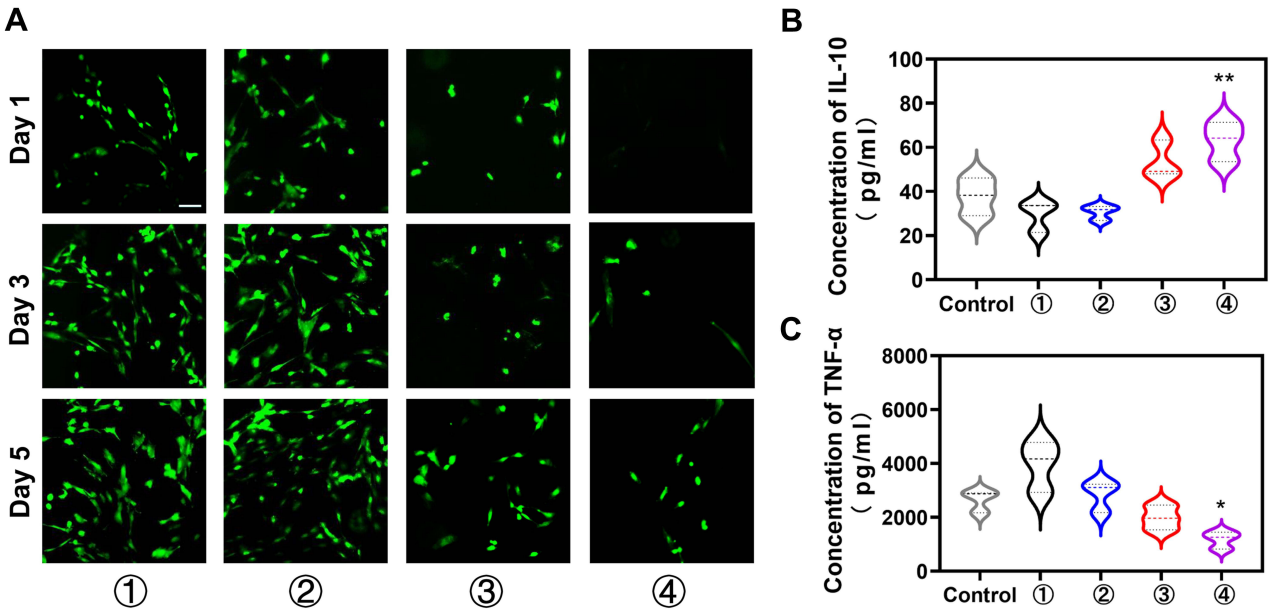

Figure 6 (**A**) The PRFs number of adhesions on each group NFm was detected by Calcein-AM/PI staining. Effects of NFm on the levels of IL-10 (**B**) and TNF-α (**C**) in activated RAW264.7 cells. *p < 0.05, **p < 0.01 vs the control. ①, PLGA NFm; ②, PLGA-g-PVP NFm; ③, PLGA-g-PVP/PC1 NFm; ④, PLGA-g-PVP/PC2 NFm. Scale bar = 200 μm.

Effect on the Inflammatory Response in vitro

The inflammatory response determines the fate of healing. M1 macrophages can stimulate the proliferation of fibroblasts by secreting proinflammatory cytokines (IL-1β, IL-6 and TNF-α), and M2 macrophages can antagonize these cytokines by secreting anti-inflammatory cytokines (IL-10).[35] Therefore, we assessed the effects of PLGA-g-PVP/PC NFm on the lipopolysaccharide-induced production of TNF-α and IL-10 in RAW264.7 cells. The results showed that PLGA-g-PVP/PC2 NFm significantly increased IL-10 (Figure 6B) and repressed TNF-α (Figure 6C). This indicated that PLGA-g-PVP/PC2 NFm might exert antiproliferative effects on fibroblasts by modulating the inflammatory response.

The Anti-Epidural Adhesion Effect in vivo

Rabbits were used to establish a laminectomy model, and epidural adhesion was evaluated by gross observation and histological analyses. The control group gradually formed epidural adhesions due to the lack of protective barriers, and the adhesion tissue was difficult to separate. In contrast to the control, Interceed effectively reduced the formation of adhesion tissue and was almost entirely degraded at 4 weeks. However, there were still a few adhesions that were difficult to separate. Excitingly, PLGA-g-PVP-PC2 NFm effectively separated the spinal dura mater and surrounding tissue and was better degraded than Interceed. There were a few adhesions, but they were observed only in the NFm margin and were easily separated (Figure 7A–D). After 4 weeks, the adhesion tissues were harvested for hematoxylin-eosin (H&E) staining, Sirius red staining, and immunohistochemistry. H&E staining showed more inflammatory cell infiltrates in the control group than in the Interceed and PLGA-g-PVP-PC2 NFm groups, which was consistent with the in vitro findings (Figure 7E). Cross-linked collagen fibers are the major component of scars,[36] and Sirius red staining was used to detect the collagen density of adhesion tissues. Sirius red staining results showed that the collagen density of adhesion tissues in the PLGA-g-PVP-PC2 NFm group was lower than that in the Interceed and control groups (Figure 7F). To detect the inflammatory response in the scar tissue of PLGA-g-PVP-PC2 NFm, the expression of TNF-α and IL-6 was visualized by immunohistochemistry. The results indicated that the TNF-α and IL-6 levels in the PLGA-g-PVP-PC2 NFm group were lower than those in the Interceed and control groups (Figure 7G and H). The above results confirmed that PLGA-g-PVP-PC2 NFm could effectively prevent the formation of epidural

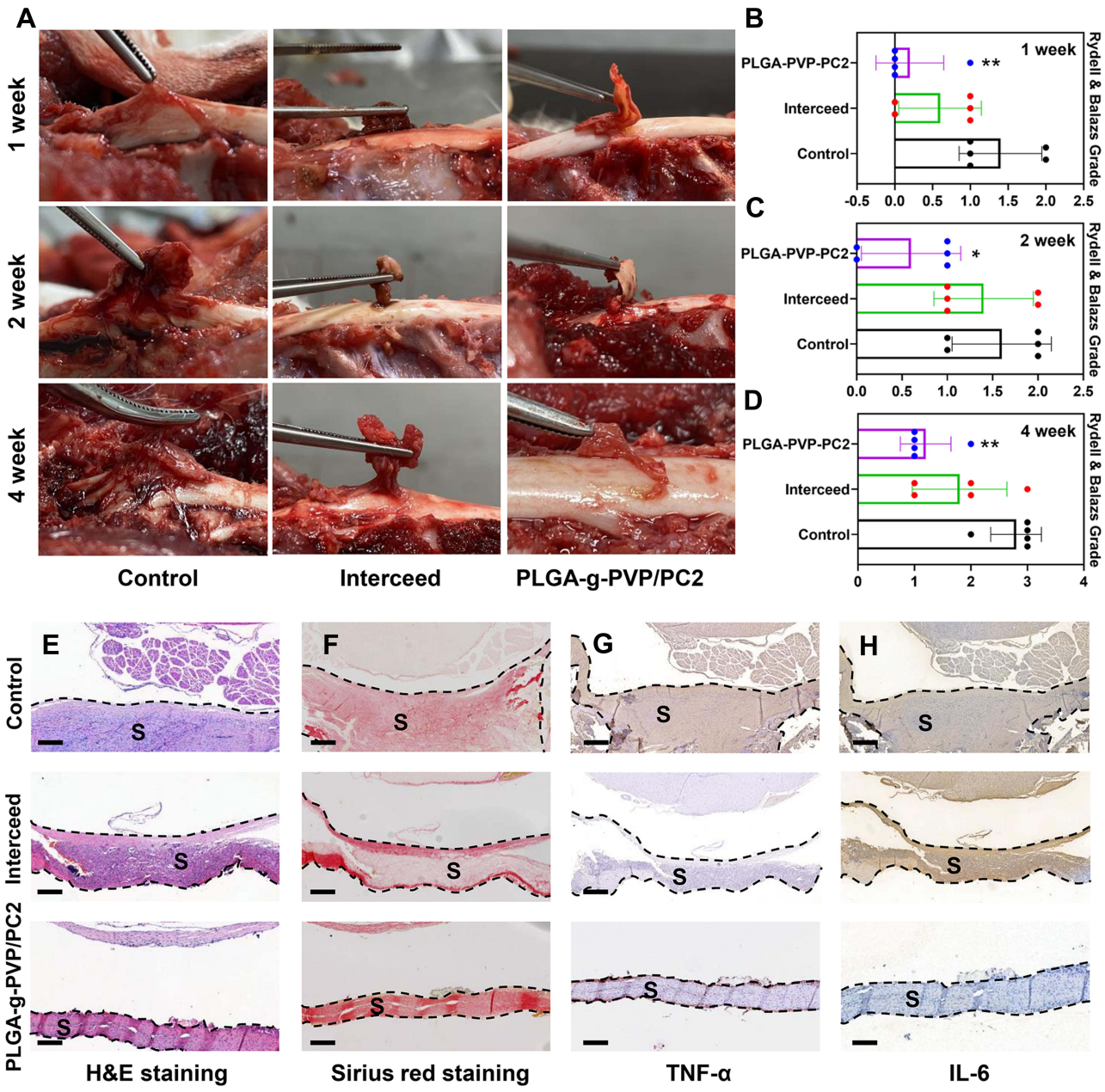

Figure 7 (**A**) Visual evaluation of adhesion status in different groups. (**B–D**) Adhesion scores in different groups. (**E**) H&E staining. (**F**) Sirius red staining. (**G**) Immunohistochemical staining analyses of TNF-α (**G**) and IL-6 (**H**). *p < 0.05, **p < 0.01 vs the control. Scale bar = 400 μm. (**S**) scar tissue.

adhesion and reduce scar adhesion. In addition, there was no obvious inflammatory response during this process, which indicated that PLGA-g-PVP-PC2 NFm was a safe and mild antiadhesion material.

Conclusion

In this study, NVPs were grafted with PLGA by 60Co to prepare PLGA-g-PVP and cross-linked to PLGA-g-PVP nanofibers and PC nanofibers by electrospinning to prepare the superhydrophilic PLGA-g-PVP/PC NFm. PLGA-g-PVP/PC NFm had extremely strong hydrophilicity and could exert anti-epidural adhesion effects without obvious inflammatory responses in vitro and in vivo. Therefore, it is a very attractive potential antiadhesion material for postoperative rehabilitation.

Institutional Review Board Statement

All animal experiments were performed according to protocols approved by the Institutional Animal Care and Use Committee (IACUC) at Sichuan University. This study was conducted in accordance with the Declaration of Helsinki and approved by the Ethics Committee of Sichuan University (Approval Number: 2020179A).

Data Sharing Statement

Data are available on request to the corresponding author.

Funding

This work was supported by China, the Sichuan Science and Technology Program (2020YFS0080, 2020YFQ0007, 2021JDRC0159), the Science and Technology Project of the Tibet Autonomous Region (XZ201901-GB-08), the 1·3·5 Project for Disciplines of Excellence, West China Hospital, Sichuan University (ZYJC21026, ZYJC21077), the Natural Science Fund of the Tibet Autonomous Region (XZ202101ZR0112G), and the Project of the Hospital of Chengdu Office of the People's Government of the Tibet Autonomous Region (2020-YJYB-1).

Disclosure

The authors declare no conflicts of interest in this work.

References

1. Frost BA, Camarero-Espinosa S, Foster EJ. Materials for the spine: anatomy, problems, and solutions. *Materials*. 2019;12(2). doi:10.3390/ma12020253
2. Song Z, Wu T, Sun J, et al. Metformin attenuates post-epidural fibrosis by inhibiting the TGF-β1/Smad3 and HMGB1/TLR4 signaling pathways. *J Cell Mol Med*. 2021;25(7):3272–3283. doi:10.1111/jcmm.16398
3. Wang W, Wang Y, Lou T, et al. Celecoxib-loaded electrospun fibrous antiadhesion membranes reduce COX-2/PGE (2) induced inflammation and epidural fibrosis in a rat failed back surgery syndrome model. *Neural Plast*. 2021;2021:6684176. doi:10.1155/2021/6684176
4. Alizadeh R, Sharifzadeh SR. Pathogenesis, etiology and treatment of failed back surgery syndrome. *Neuro Chirurgie*. 2021. doi:10.1016/j.neuchi.2021.09.005
5. Xue J, Wu T, Dai Y, Xia Y. Electrospinning and electrospun nanofibers: methods, materials, and applications. *Chem Rev*. 2019;119(8):5298–5415. doi:10.1021/acs.chemrev.8b00593
6. Choi Y, Park MH, Lee K. Tissue engineering strategies for intervertebral disc treatment using functional polymers. *Polymers*. 2019;11(5):872. doi:10.3390/polym11050872
7. Yu CC, Chen YW, Yeh PY, et al. Random and aligned electrospun PLGA nanofibers embedded in microfluidic chips for cancer cell isolation and integration with air foam technology for cell release. *J Nanobiotechnology*. 2019;17(1):31. doi:10.1186/s12951-019-0466-2
8. Zhu S, Xing H, Gordiichuk P, Park J, Mirkin CA. PLGA spherical nucleic acids. *Adv Mater*. 2018;30(22):e1707113. doi:10.1002/adma.201707113
9. Hu Q, Xia X, Kang X, et al. A review of physiological and cellular mechanisms underlying fibrotic postoperative adhesion. *Int J Biol Sci*. 2021;17(1):298–306. doi:10.7150/ijbs.54403
10. Luengo J, Schneider M, Schneider AM, Lehr CM, Schaefer UF. Human skin permeation enhancement using PLGA nanoparticles is mediated by local pH changes. *Pharmaceutics*. 2021;13(10):1608. doi:10.3390/pharmaceutics13101608
11. Zwicky SN, Stroka D, Zindel J. Sterile injury repair and adhesion formation at serosal surfaces. *Front Immunol*. 2021;12:684967. doi:10.3389/fimmu.2021.684967
12. Li AD, Sun ZZ, Zhou M, et al. Electrospun Chitosan-graft-PLGA nanofibres with significantly enhanced hydrophilicity and improved mechanical property. *Colloids Surf B Biointerfaces*. 2013;102:674–681. doi:10.1016/j.colsurfb.2012.09.035
13. Foraida ZI, Kamaldinov T, Nelson DA, Larsen M, Castracane J. Elastin-PLGA hybrid electrospun nanofiber scaffolds for salivary epithelial cell self-organization and polarization. *Acta Biomaterialia*. 2017;62:116–127. doi:10.1016/j.actbio.2017.08.009
14. Kazemi L, Rahbarghazi R, Salehi R, et al. Superior synaptogenic effect of electrospun PLGA-PEG nanofibers versus PLGA nanofibers on human neural SH-SY5Y cells in a three-dimensional culture system. *J Mol Neurosci*. 2020;70(12):1967–1976. doi:10.1007/s12031-020-01596-7
15. Wu K, Shiu BC, Zhang D, et al. Preparation of nanoscale urushiol/PAN films to evaluate their acid resistance and protection of functional PVP films. *Nanomaterials*. 2021;11(4). doi:10.3390/nano11040957
16. Wang J, Chen H, Chen Z, et al. In-situ formation of silver nanoparticles on poly (lactic acid) film by γ-radiation induced grafting of N-vinyl pyrrolidone. *Mater Sci Eng C Mater Biol Appl*. 2016;63:142–149. doi:10.1016/j.msec.2016.01.077
17. Wang J, Peng C, Chen Z, et al. Engineering antimicrobial and biocompatible electrospun PLGA fibrous membranes by irradiation grafting polyvinylpyrrolidone and periodate. *Colloids Surf B Biointerfaces*. 2019;181:918–926. doi:10.1016/j.colsurfb.2019.06.059
18. Tsaousi G, Stavrou G, Fotiadis K, Kotzampassi K, Kolios G. Implementation of phospholipids as pharmacological modalities for postoperative adhesions prevention. *Eur J Pharmacol*. 2019;842:189–196. doi:10.1016/j.ejphar.2018.10.054
19. Li D, Mao C, Zhou E, et al. MicroRNA-21 mediates a positive feedback on angiotensin II-induced myofibroblast transformation. *J Inflamm Res*. 2020;13:1007–1020. doi:10.2147/jir.S285714
20. Wang J, Yang L, You J, et al. Platelet-derived growth factor regulates the biological behavior of oral mucosal fibroblasts by inducing cell autophagy and its mechanism. *J Inflamm Res*. 2021;14:3405–3417. doi:10.2147/jir.S313910

21. Dandamudi M, McLoughlin P, Behl G, et al. Chitosan-coated PLGA nanoparticles encapsulating triamcinolone acetonide as a potential candidate for sustained ocular drug delivery. *Pharmaceutics*. 2021;13(10):1590. doi:10.3390/pharmaceutics13101590
22. Ravikiran T, Anand S, Ansari MA, et al. Fabrication and in vitro evaluation of 4-HIA encapsulated PLGA nanoparticles on PC12 cells. *Int J Nanomed*. 2021;16:5621–5632. doi:10.2147/ijn.S317986
23. Wu K, Zhang D, Liu M, Lin Q, Shiu BC. A study on the improvement of using raw lacquer and electrospinning on properties of PVP nanofilms. *Nanomaterials*. 2020;10(9). doi:10.3390/nano10091723
24. Yang X, Wang X, Chen XY, et al. Pinocembrin¯lecithin complex: characterization, solubilization, and antioxidant activities. *Biomolecules*. 2018;8 (2):41. doi:10.3390/biom8020041
25. Kim HG, Lee US, Kwac LK, et al. Electron beam irradiation isolates cellulose nanofiber from Korea ”tall goldenrod” invasive alien plant pulp. *Nanomaterials*. 2019;9(10). doi:10.3390/nano9101358
26. Masters EA, Trombetta RP, de Mesy Bentley KL, et al. Evolving concepts in bone infection: redefining ”biofilm”, ”acute vs. chronic osteomyelitis”, ”the immune proteome” and ”local antibiotic therapy”. *Bone Res*. 2019;7(1):20. doi:10.1038/s41413-019-0061-z
27. Gurtner GC, Werner S, Barrandon Y, Longaker MT. Wound repair and regeneration. *Nature*. 2008;453(7193):314–321. doi:10.1038/nature07039
28. Fatehi Hassanabad A, Zarzycki AN, Jeon K, Deniset JF, Fedak PWM. Post-operative adhesions: a comprehensive review of mechanisms. *Biomedicines*. 2021;9(8):867. doi:10.3390/biomedicines9080867
29. Morton LM, Phillips TJ. Wound healing and treating wounds: differential diagnosis and evaluation of chronic wounds. *J Am Acad Dermatol*. 2016;74(4):589–605. doi:10.1016/j.jaad.2015.08.068
30. Hsu SH, Dai LG, Hung YM, Dai NT. Evaluation and characterization of waterborne biodegradable polyurethane films for the prevention of tendon postoperative adhesion. *Int J Nanomed*. 2018;13:5485–5497. doi:10.2147/ijn.S169825
31. Eming SA, Martin P, Tomic-Canic M. Wound repair and regeneration: mechanisms, signaling, and translation. *Sci Transl Med*. 2014;6 (265):265sr266. doi:10.1126/scitranslmed.3009337
32. Zahran SME, Abdel-Halim AH, Nassar K, Nada AA. Fabrication of nanofiltration membrane based on non-biofouling PVP/lecithin nanofibers reinforced with microcrystalline cellulose via needle and needle-less electrospinning techniques. *Int J Biol Macromol*. 2020;157:530–543. doi:10.1016/j.ijbiomac.2020.04.152
33. Kopeć K, Wojasiński M, Ciach T. Superhydrophilic polyurethane/polydopamine nanofibrous materials enhancing cell adhesion for application in tissue engineering. *Int J Mol Sci*. 2020;21(18):6798. doi:10.3390/ijms21186798
34. Zangi S, Hejazi I, Seyfi J, et al. Tuning cell adhesion on polymeric and nanocomposite surfaces: role of topography versus superhydrophobicity. *Mater Sci Eng C Mater Biol Appl*. 2016;63:609–615. doi:10.1016/j.msec.2016.03.021
35. Xu X, Gu S, Huang X, et al. The role of macrophages in the formation of hypertrophic scars and keloids. *Burns Trauma*. 2020;8:tkaa006. doi:10.1093/burnst/tkaa006
36. Wilkinson HN, Hardman MJ. Wound healing: cellular mechanisms and pathological outcomes. *Open Biol*. 2020;10(9):200223. doi:10.1098/rsob.200223